A numerical and experimental approach in understanding the performance of textured surfaces in sliding contacts

A Numerical and Experimental Approach in Understanding the Performance of Textured Surfaces in Sliding Contacts

Nicholas J. Morris*, Miguel De la Cruz, Ramin Rahmani, Michael Leighton, Homer Rahnejat and Paul King
Wolfson school of Mechanical and Manufacturing Engineering, Loughborough University,
Loughborough, LE11 3TU, United Kingdom

*Corresponding author: N.J.Morris@Lboro.ac.uk

1. Introduction

The piston compression ring-bore contact accounts for 5-6% of input fuel energy [1]. This is significant for such a small conjunction. With ever-increasing costs and stricter emerging legislation much attention is directed towards reducing the parasitic losses.
The piston ring is one of the most challenging tribological contacts on account of transient nature of the regime of lubrication during a typical engine cycle [2]. High friction occurs at piston reversals at the top and bottom dead centres, with highest friction at the beginning of the power stroke, where high pressures act behind the inner rim of the ring and with low piston sliding speed, inducing some Boundary interactions [2]. Laser texturing is used to reduce friction [3-7].
This paper comprises direct measurement of friction from a reciprocating slider bearing test rig. It also presents numerical prediction of the same. The combined approach enables the study of possible improvements in tribological conditions similar to ring reversals in a piston system, but at a more fundamental level. It further reduces a plethora of other effects such as ring dynamics [8] and thermal distortions which make measurements difficult in an operating engine.

2. Experimental method

A reciprocating slider bench test rig is developed [9]. A sliding thin strip (representative of compression ring thickness) with a face-width profile is loaded against and slides upon a flat plate. The plate is mounted upon precision low friction bearings and is allowed to float, when dragged by the sliding strip. An electric motor is directly coupled to the loaded and sliding strip via low friction and an almost backlash-free leadscrew. Piezo-resistive force sensors measure the inertial force of the floating plate, which is due to generated contact friction as:

$$\sum F = -F_t = ma \qquad (1)$$

A Rotational Laser Doppler Vibrometer is used to record the actual speed of the sliding strip.

The thin strip is made of stainless steel 330 C and is hardened to 62HRC. The flat plate is made of EN 14 steel, electroplated by a 20µm thick Ni-SiC coating. The surface is then ground and polished (Table 2).

2.1 Laser surface texturing

Chevron-shaped textures were laser etched onto a region of the floating plate. A SPI 200Watt Fibre laser was used to create the chevrons. The laser parameters are provided in Table 1.

Table 1. Laser data

Parameter	Value (Unit)
Beam Width	0.030 (mm)
Feed speed	0.25 (mm/s)
Pulse Width	0.500 (ms)
Frequency	1687 (Hz)
Power	16 (W)
Shielding Gas	Nitrogen @ 0.5 MPa

After the LST process, the plate is polished again for a short period of time to remove any splatter or debris left protruding from the surface. Figure 1 shows an image of typical laser-etched chevrons obtained through Alicona Infinite Focus Microscope.

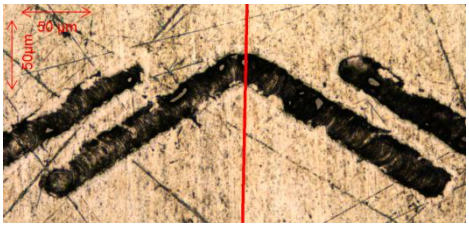

Figure 1: Image of chevrons on test plate

Surface roughness was measured for the plate the strip. In addition the chevron depth and ring face profile were also measured. The chevrons have a thickness-to-depth ratio of 0.11 (representative of an optimised ratio as demonstrated in [3]) although some variation in the chevron depth is produced in the laser surface texturing process.

The laser surface texturing produces chevrons with a cross-sectional profile similar to that of a parabola (figure 2), therefore, modelled accordingly.

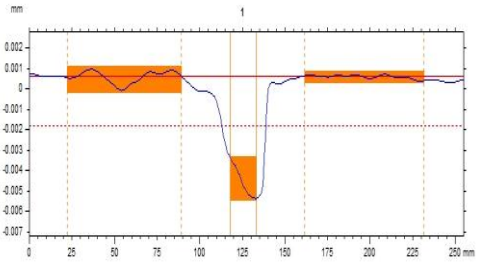

Figure 2: A typical produced chevron profile

If l is a typical chevron's cross-sectional width, h_d is the depth of the chevron at its centre and x_0 its centre position, then the profile can be described by:

$$\left(\frac{x-x_0}{l/2}\right)^2 + \frac{y}{h_d} = 1 \qquad (2)$$

2.2 Test protocol

The load cells were calibrated before each set of tests. The contacting surface topography of the strip and the floating plate specimen were measured. Figure 3 shows typical topography of the strip's contacting face-width. The strip and the floating plate specimen were then mounted onto the test rig and proper alignment was ensured. A drop of oil was applied to the flat liner plate using a syringe. The oil was evenly spread across the surface. An initial running-in period was allowed prior to each test. After each test the surfaces of the strip and the floating plate were measured again.

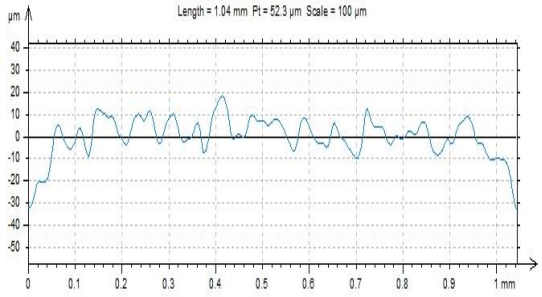

Figure 3: Measured ring face

3. Numerical method

A combined numerical and experimental approach is undertaken to ascertain the effectiveness of laser textured surfaces in retention of lubricant film and improve hydrodynamic load carrying capacity, as well as reducing friction. Previous experimental evidence has suggested that in the case of piston-cylinder system 2-4% reduction in friction is attained [5,6]. Furthermore, Balakrishnan et al [10] carried out numerical analysis for piston skirt-cylinder bore conjunction and showed improved oil retention through creation of textured chevron-type reservoirs at the top dead centre. Their results agreed with oil film thickness measurement using ultrasonic sensors by Dwyer-Joyce et al [11]. However, measurements of either oil film thickness or friction were not obtained for the much narrower ring-bore conjunction. This paper uses a thin strip slider, representing a segment of circumferentially conforming ring against a flat floating plate of finite width. A 2D analysis can be carried out, using Reynolds equation:

$$\frac{\partial}{\partial x}\left(\frac{\rho h^3}{6\eta}\frac{\partial p}{\partial x}\right)+\frac{d}{dy}\left(\frac{\rho h^3}{6\eta}\frac{\partial p}{\partial y}\right)=(U_1-U_2)\frac{\partial}{\partial x}(\rho h)+2\frac{\partial}{\partial t}(\rho h) \quad (3)$$

Reynolds equation is solved together with the film thickness equation, representing the gap shape:

$$h(x,y,t)=h_0(t)+h_s(x,y)+h_t(x,y) \quad (4)$$

where, h_0 is the minimum film thickness, h_s is the ring face profile and h_t describes the profiles of surface features, i.e. chevrons in this study.

The ring face-width profile $h_s$is measured, and only varies in the x-direction (direction of entraining motion).

For the purpose of numerical analysis, the film profile in figure 4 is created using the following set of equations.

$$h_s(x)=\begin{Bmatrix}-sx+g & if\ \ x\le q\\ 0 & if\ \ q<x<r\\ sx-g & if\ \ x\ge r\end{Bmatrix} \quad (5)$$

where, s is the gradient with respect to ring face-width, g is the film profile at x=0 (the intercept) and r and q refer to the edge and flat land film shape.

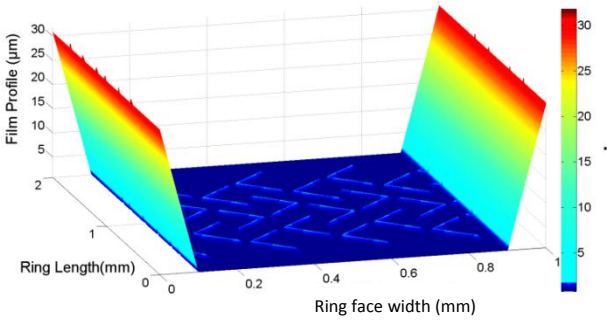

Figure 4: Film Shape with chevrons

As the result of relatively low applied load, there is no localised deflection of the contacting surfaces and a hydrodynamic regime of fluid film lubrication is expected. The combination of low load and low lubricant entrainment simulates load-kinematic conditions at TDC reversals under assumed isothermal conditions (such as cold start-up or motored engines). Solution of equations (3) and (4) yields the lubricant film thickness and the hydrodynamic load carrying capacity as:

$$W_h=\int_0^l\int_0^b p\,dxdy \quad (6)$$

A fully flooded inlet is assumed as the surface of the *floating* plate is provided with a layer of free surface film ahead of the sliding contact. However, low sliding speed is often insufficient to entrain a volume of lubricant into the contact. Thus, a mixed regime of lubrication is anticipated. The outlet boundary conditions are those of Swift-Stieber [2] with assumed atmospheric vaporisation pressure at the film rupture point .The inlet pressure at the front face of the strip is set to atmospheric pressure. Only a segment of the whole strip width in the y-direction (direction of lubricant side-leakage) was included in the model to keep the computational time to an acceptable level. Therefore, symmetric boundary conditions in the transverse direction are used. Thus, the boundary conditions are:

$$p=p_{in}\quad at\quad x=-b/2 \quad (7)$$

$$p=p_c,\ \frac{dp}{dx}=0\quad at\quad x=x_c \quad (8)$$

$$\left.\frac{\partial p}{\partial y}\right|_{(x,0)}=\left.\frac{\partial p}{\partial x}\right|_{(x,l)}=0 \quad (9)$$

As already noted, with slider-type rigs and at low sliding speeds there is some degree of asperity interactions. To account for the appearance of mixed and/or boundary regimes of lubrication at reversals, Greenwood and Tripp [12] asperity contact model was employed. The load carried by the asperities is given by equation (10), where E' is the composite Young's modulus of elasticity of the contacting surfaces, and

$\zeta k\sigma$ and σ/k are the roughness parameters.

$$W_a = \frac{16\sqrt{2}}{15}\pi(\zeta k\sigma)^2\sqrt{\frac{\sigma}{k}}E'AF_{5/2}(\lambda) \quad (10)$$

and the statistical function takes the following form

$$F_j(\lambda) = \frac{1}{2\pi}\int_\lambda^\infty (s-\lambda)^j exp\left(-\frac{s^2}{2}\right)ds \quad (11)$$

The sum of the viscous and asperity loads gives the load carrying capacity as:

$$W_T = W_h + W_a \quad (12)$$

The convergence criterion for the numerical analysis is the load balance; between the applied load and that carried by the contact as:

$$\frac{|F-W_T|}{F} \leq \varepsilon \quad (13)$$

where, F is the applied load and ε is the error tolerance.

An iterative procedure is followed, if the criterion is not met, by altering the initially guessed value of h_0.

The generated viscous friction is given as:

$$F_v = \int_0^l\int_0^b \tau\, dxdy \quad (14)$$

Where, assuming no side leakage:

$$\tau = -\frac{h}{2}\frac{\partial p}{\partial x} + \frac{\eta(U_1-U_2)}{h} \quad (15)$$

Boundary friction contribution comprises two parts, as it is assumed that a thin layer of absorbed lubricant resides on the asperity summits and acts in accordance with the non-Newtonian Eyring shear stress τ_0. There is also boundary shear strength of cold-welded asperity pairs on the contiguous counterfaces; ξ, which for a ferrous oxide layer has the value of 0.17 [13].

$$F_b = \tau_0 A_a + \xi W_a \quad (16)$$

The asperity contact area A_a for typical asperity geometry and assumed Gaussian distribution can be obtained from equation (17) considering the general form of statistical function, $F_2(\lambda)$ as [11]:

$$A_a = \pi^2(\zeta k\sigma)^2 AF_2(\lambda) \quad (17)$$

The total friction becomes:

$$F_t = F_v + F_b \quad (18)$$

4. Results

The numerical results are obtained based on the data given in Table 2. The sliding speed is measured as described above. Its mean value is 24.42 mm/s (±0.06 mm/s).

Table 2. Parameters used in numerical analysis

Parameter	Value
Lubricant viscosity (Pa.s)	0.1583
Ring face width (mm)	1
Ring surface roughness (μm) Ra, Rq	0.511, 0.709
Liner surface roughness (μm) Ra, Rq	0.172, 0.105
Stroke length (mm)	80 (max)
Applied load (N)	0.8
Ring length (mm)	32

The generated pressure distribution is shown in Figure 5. The pressure profile has two distinct features. There is a wedge effect and a trough at the inlet to each chevron facing lubricant entrainment. These act as reservoirs, thus causing low pressure regions. For the chevrons facing opposite to the direction of entrainment there is sharp rise in generated pressures (pressure perturbation). These pressure perturbations are reminiscent of micro-elastohydrodynamic effect such as those caused by rough cartilage in endo-articular joints. Pressure fluctuations enhance load carrying capacity of the contact relative to the nominally smooth surface.

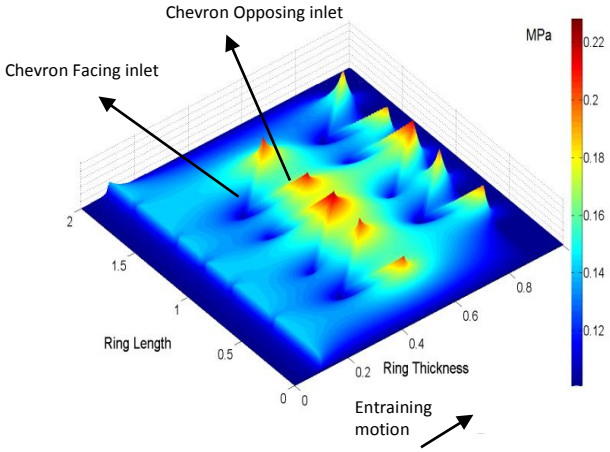

Figure 5: Viscous pressure distribution

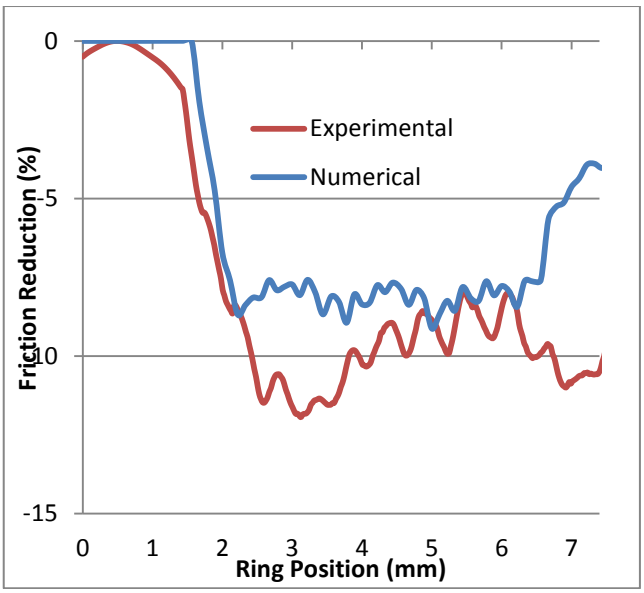

Figure 6: Predicted and measured reduced friction with chevron textures

Therefore, as the strip traverses the introduced chevrons

an increase in the load carrying capacity is predicted. Hence, at the constant applied load, this effect translates to increased film thickness, hence reduced friction as evident from both experimental measurement and numerical predictions (figure 6). This figure provides percentage friction reduction in the textured region with respect to the untreated part of the plate surface. Good qualitative and quantitative comparison is noted between measurements and predictions.

5. Acknowledgement

This research is sponsored by the Engineering and Physical Sciences Council (EPSRC) under the Encyclopaedic Program Grant.

6. References

[1] Andersson BS. "Company's perspective in vehicle tribology" in Dowson D, Taylor CM, Godet M, editors. Proc. 18th Leeds-Lyon Sympos. Elsevier; 1991, pp. 503-506.

[2] Gohar, R. and Rahnejat, H., "Fundamentals of Tribology", Imperial College Press, London, 2008

[3] Etsion, I., and E. Sher. "Improving fuel efficiency with laser surface textured piston rings." Tribology International 42.4 (2009): 542-547.

[4] Ryk, G., Kligerman, Y. and Etsion, I. "Experimental Investigation of Laser Surface Texturing for Reciprocating Automotive Components", Trib. Trans., 45, 2002, pp. 444-449

[5] Rahnejat, H., Balakrishnan, S., King, P.D. and Howell-Smith, S., "In-cylinder friction reduction using a surface finish optimisation technique", Proc. IMechE, Part D: J. Automobile Engineering, 220, 2006, pp. 1309-1318

[6] Etsion, I., "Surface Texturing for In-Cylinder Friction Reduction", in Rahnejat, H. (Ed.) Tribology and Dynamics of Engine and Powertrain, Woodhead Publishing, Cambridge, 2010

[7] Ronen, A., Etsion, I., and Kligerman, Y., "Friction-Reducing surface texturing in reciprocating automotive components", Trib. Trans 44, 2001, pp. 359-366

[8] Baker, C.E., Theodossiades, S., Rahnejat, H. and Fitzsimons, B., "Influence of in-plane dynamics of thin compression rings on friction in internal combustion engines", J. Engineering for Gas Turbines & Power, 134, 092801-1

[9] De la Cruz, M., Gore, M., Morris, N. and Rahnejat, H. "The role of laser surface textured patterns on friction in reciprocating contacts", Proc. ASME/STLE 2012 International Joint Tribology Conference, IJTC2012:61149, 2012, Denver, Colorado.

[10] Balakrishnan, S., Howell-Smith, S. and Rahnejat, H., "Investigation of reciprocating conformal contact of piston skirt-to-surface modified cylinder liner in high performance engines", Proc. IMechE, J. Mech. Engineering Science, 219, 2005, pp. 1235-1247

[11] Dwyer-Joyce, R.S., Green, D.A., Balakrishnan, S., et al., "The measurement of liner-piston skirt oil film thickness by an ultrasonic means", SAE Int., Technical Pap.: 2006-01-0648, 2006

[12] Greenwood J.A. and Tripp J.H., "The contact of two nominally flat rough surfaces", Proc. IMechE, 185, 1970–1971, pp. 625–634.

[13] Teodorescu M, Kushwaha M, Rahnejat H. and Rothberg, S.J., "Multi-physics analysis of valve train systems: from system level to micro-scale interactions", Proc. IMechE, Part K: J Multi-body Dynamics, 221, 2007, pp. 349–360.

Nomenclature

A	Apparent Contact Area
A_a	Asperity Contact Area
b	Ring Face Width
E'	Effective Elastic modulus of the contacting pair
f_b	Boundary Friction
f_t	Total Friction
f_v	Viscous Friction
h	Film Thickness
h_0	Minimum Film thickness
h_s	Profile of the ring face width
h_t	Surface Feature film thickness
h_d	Chevron Height
l	Ring Length
l_c	Chevron thickness
p	Pressure
p_c	Cavitation Pressure
p_{in}	Inlet Pressure
q,r,f,g,s	Ring profile co-efficients
t	Time
U_1, U_2	Ring, liner speed of entraining motion
V_1,V_2	Ring, liner speed in the axial direction
W_a	Load share of asperities
W_h	Hydrodynamic Load share
W_T	Total load carried
x	Direction along the ring face(in the direction of entraining motion)
x_c	Film rupture boundary
x_m	Centre or the chevron at each cross section
y	Direction axially along the ring

Greek Symbols

η	Lubricant dynamic viscosity
κ	Average Asperity tip
λ	Stribeck oil film parameter
ρ	Lubricant Density